



Title	Histopathological changes in tear-secreting tissues and cornea in a mouse model of autoimmune disease
Author(s)	Masaya, Hiraishi; Md Abdul, Masum; Takashi, Namba; Otani, Yuki; Elewa, Yaser H. A.; Ichii, Osamu; Kon, Yasuhiro
Citation	Experimental Biology and Medicine, 245(12), 999-1008 https://doi.org/10.1177/1535370220928275
Issue Date	2020-06-01
Doc URL	http://hdl.handle.net/2115/79023
Rights	Masaya Hiraishi, Md Abdul Masum, Takashi Namba, Yuki Otani, Yaser HA Elewa, Osamu Ichii, Yasuhiro Kon, Histopathological changes in tear-secreting tissues and cornea in a mouse model of autoimmune disease, Experimental Biology and Medicine (Volume 245 Issue 12) pp. 999-1008. Copyright © 2020 the Society for Experimental Biology and Medicine (SEBM). DOI: 10.1177/1535370220928275
Type	article (author version)
Additional Information	There are other files related to this item in HUSCAP. Check the above URL.
File Information	Manuscript.pdf



[Instructions for use](#)

1 **Histopathological changes in tear-secreting tissues and cornea in a mouse model of**
2 **autoimmune disease**

3

4 **Short title: Histopathology of tear-secreting tissues**

5

6 Masaya Hiraishi^{1*}, Md. Abdul Masum^{1,2*}, Takashi Namba¹, Yuki Otani¹, Yaser Hosny Ali
7 Elewa^{1,3}, Osamu Ichii^{1,4#}, and Yasuhiro Kon¹.

8 ^{1.} Laboratory of Anatomy, Department of Basic Veterinary Sciences, Faculty of Veterinary
9 Medicine, Hokkaido University, Sapporo, 060-0618, Japan

10 ^{2.} Department of Anatomy, Histology and Physiology, Faculty of Animal Science and
11 Veterinary Medicine, Sher-e-Bangla Agricultural University, Dhaka, 1207, Bangladesh

12 ^{3.} Department of Histology, Faculty of Veterinary Medicine, Zagazig University, Zagazig,
13 44519, Egypt

14 ^{4.} Laboratory of Agrobiomedical Regenerative Medicine, Faculty of Agriculture, Hokkaido
15 University, Sapporo, 060-8589, Japan

16

17 * Hiraishi M and Masum MA equally contributed to this paper

18 # Corresponding author:

19 Osamu Ichii, DVM, PhD

20 Laboratory of Anatomy, Department of Basic Veterinary Sciences, Faculty of Veterinary
21 Medicine, Hokkaido University, Kita 18, Nishi 9, Kita-ku, Sapporo 060-0818, Japan

22 Email: ichi-o@vetmed.hokudai.ac.jp

23 Tel: +81-11-706-5189, Fax: +81-11-706-5189

24 **Abstract**

25 The tear film covers the cornea, and its abnormalities (including immunological) induce dry
26 eye. Using autoimmune disease model mice, BXSB/MpJ-*Yaa* (BXSB-*Yaa*), histopathological
27 changes in the eye and tear-secreting tissues were examined using histopathology,
28 immunohistochemistry, and electron microscopy at 8, 20, and 28 weeks for early, middle, and
29 late disease stages. Early and middle stage BXSB-*Yaa* showed increased serum autoantibody
30 and spleen to body weight (S/B), respectively, and higher tear volume than controls, BXSB/MpJ
31 (BXSB), at early stages, which decreased with ageing and negatively correlated with
32 autoimmune disease indices. Late stage BXSB-*Yaa* showed smaller Meibomian gland acini, less
33 intraorbital lacrimal gland, and smaller Harderian gland acinar cells than BXSB; the latter two
34 indices decreased with ageing and negatively correlated with S/B. Cell infiltration occurred in
35 the middle stage BXSB-*Yaa* extraorbital lacrimal gland, and acinar cells were smaller than
36 BXSB. The conjunctiva goblet cells decreased from early to middle stages in both strains, but in
37 BXSB-*Yaa*, they increased at late stages with a partial lack of microvilli on the cornea and were
38 inversely altered with anterior epithelium thickness through ageing, suggesting that they
39 compensated for anterior epithelium damage. In conclusion, the tear film was unstable due to an
40 autoimmune disease condition in BXSB-*Yaa*.

41

42 **Keywords**

43 Tear film, Cornea, Autoimmune disease, BXSB/MpJ-*Yaa* mice

44 **Impact statement**

45 Cornea, an outermost layer of mammalian eye, is protected by tear film and abnormalities of
46 tear film causes dry eye. Dry eye injures the cornea which results lower vision in patients.
47 Several factors cause dry eye, including altered systemic conditions, environment, and
48 immunological abnormality of the patient in autoimmune disease like Sjögren's syndrome (SS).
49 However, the detailed pathology of autoimmune abnormality-mediated dry eye is unclear. Here
50 we demonstrated that systemic autoimmune abnormality in BXSB-Yaa mice was associated
51 with histological changes in the exocrine glands and cornea of the eyes. We also showed that
52 BXSB-Yaa mice developed mild or early stage dry eye-like disease and explain the existence of
53 a compensatory mechanism associated with the dysfunction of these tissues. Thus, BXSB-Yaa
54 could be a model for SS-like disease-associated dry eye and these data would contribute to the
55 understanding of the pathogenesis of autoimmune-related dry eye disease.

56

57 **Introduction**

58 For mammalian eyeballs, the outermost cornea is covered and protected by the tear film
59 composed of mucin, water, and lipid layers from its inner side. Secretions from conjunctival
60 goblet cells, lacrimal glands (LGs), and the Meibomian gland (MG) contribute to the formation
61 of the tear film.¹⁻³ The deep gland of the third eyelid, known as the Harderian gland (HG), also
62 contributes to the formation of the lipid layer.⁴ Dysfunction or injuries in these tear film-forming
63 cells cause several eye diseases. Loss of conjunctival goblet cells and dysfunction of the LG as
64 well as the MG causes the disruption of the water layer, since the latter is crucial to prevent the
65 evaporation of water.⁵⁻⁷ In general, eye diseases due to tear film abnormalities are diagnosed as
66 “dry eye” in humans and animals.

67 Dry eye injures the cornea in humans and companion animals; model animals of dry eye
68 have been reported.⁸⁻¹⁰ This disease reduces the quality of life in patients because it causes
69 fatigue or pain of the eyes and eventually leads to low vision. Dry eye is known as a chronic
70 disease associated with keratoconjunctivitis. Several factors cause dry eye, including altered
71 systemic conditions, environment, ophthalmic operation, and an immune abnormality of the
72 patient.¹¹⁻¹⁴ Sjögren’s syndrome (SS), a representative autoimmune disease targeting exocrine
73 glands, causes dry eye in humans.¹⁵ Between 0.04 and 3.1 million adults suffer from SS in the
74 United States.¹⁶ While SS is not fatal, approximately 5% of patients with long-term SS develop
75 malignant lymphoma.¹⁷⁻¹⁹ Companion dogs that show dry eye associated with an autoimmune
76 disorder have SS-like disease.^{20,21} For dry eye in SS, autoimmune abnormality-associated
77 inflammation in the LGs, MG dysfunction, and goblet cell loss are reported in human patients
78 and model animals.²²⁻²⁷ SS model mice have inflammation in the HG.²⁸ In Japan, SS is
79 diagnosed in patients exhibiting more than two of the following characteristics: lymphocyte
80 infiltration in labial salivary glands or LGs; hyposalivation; hyposalivation of tear fluid
81 or an injured cornea; and anti-Ro/SS-A and anti-La/SS-B antibodies in the serum.

82 To elucidate the pathology of SS, the use of an animal model is crucial. The BXSB/MpJ-
83 *Yaa* (BXSB-*Yaa*) mouse, carrying the Y-linked autoimmune accelerator (*Yaa*) mutation on the Y
84 chromosome, is a representative autoimmune disease model and develops severe symptoms,
85 including abnormal proliferation of B-cells, autoantibody production, splenomegaly, and
86 glomerulonephritis.²⁹⁻³¹ BXSB-*Yaa* manifests SS-like symptoms, such as B-cell predominant
87 lymphocytic infiltrations and the destruction of acini in extraorbital lacrimal glands (ELGs).²² In
88 that study, there was no significant difference in the quantity of tear production between BXSB-
89 *Yaa* and healthy C57BL/6 mice, suggesting that BXSB-*Yaa* could be a model for mild or early
90 stage dry eye. However, the detailed pathology of autoimmune abnormality-mediated dry eye is
91 unclear since no study has elucidated the histopathological changes in tear-secreting tissues
92 using SS model mice.

93 We investigated the histopathology of tear-secreting tissues and cornea in BXSB-*Yaa* mice,
94 evaluating autoimmune disease development and tear production by comparing them to the
95 healthy control strain BXSB/MpJ (BXSB). We found that BXSB-*Yaa* mice developed mild or
96 early stage dry eye-like disease and discuss the existence of a compensatory mechanism
97 associated with the dysfunction of these tissues in this model. These data contribute to the
98 understanding of the pathogenesis of autoimmune-related dry eye disease.

99 **Materials and Methods**

100 *Animals*

101 Male BXSB and BXSB-Yaa mice aged 8, 20, 24, and 28 weeks were purchased from Japan
102 SLC, Inc. (Hamamatsu, Japan) and maintained under specific pathogen-free conditions. Animal
103 experimentation was approved by the Institutional Animal Care and Use Committee of the
104 Faculty of Veterinary Medicine, Hokkaido University (approval No. 16-0124). All experimental
105 animals were handled in accordance with the Guide for the Care and Use of Laboratory
106 Animals, Faculty of Veterinary Medicine, Hokkaido University (approved by the Association
107 for Assessment and Accreditation of Laboratory Animal Care International).

108

109 *Sample collection*

110 Under deep anaesthesia, using a mixture of medetomidine (0.3 mg/kg), midazolam (4
111 mg/kg), and butorphanol (5 mg/kg), tears were collected using Schirmer test paper (Schirmer
112 Tear Production Measuring Strips; Showa Yakuhin, Tokyo, Japan), which was sliced at
113 approximately 1 mm width and inserted into the lower conjunctival sac for 4 min. Then, blood
114 was collected from the femoral arteries, and all mice were euthanized by cervical dislocation.
115 The heads, eyeballs, periocular tissues, and spleens were immediately collected and used for
116 further analysis.

117

118 *Tear volume measurement*

119 Tear volume was measured according to a previous report.²² Briefly, using a digital image,
120 the tear-wetted area of Schirmer test paper was measured using ImageJ (NIH,
121 <http://rsbweb.nih.gov/ij/>) and estimated as the tear volume.

122

123 *Serological analysis*

124 Serum levels of anti-double-stranded DNA (dsDNA) antibody were measured to evaluate

125 systemic autoimmune conditions and disease development using the LBIS Anti-dsDNA-Mouse
126 ELISA Kit (FUJIFILM Wako Pure Chemical Corporation; Osaka, Japan) according to the
127 manufacturer's instructions.

128

129 *Histopathological analysis*

130 The eyeballs with conjunctiva, MG, and HG were fixed with 4% paraformaldehyde (PFA)
131 at 4 °C overnight. The tissues were dehydrated using alcohol and embedded in paraffin, cut into
132 3- μ m-thick sections, and stained with haematoxylin-eosin (HE). Sections of the eyeball with
133 conjunctiva were stained with periodic acid-Schiff (PAS). The skulls including intraorbital
134 lacrimal gland (ILG), and ELG were immersed in acetone overnight to eliminate lipids after
135 fixation with 4% PFA. Then, they were immersed in 10% formic acid for 12 h to decalcify.
136 Paraffin sections (3- μ m-thick) were prepared and stained with HE or PAS.

137

138 *Histoplanimetry*

139 HE-stained sections were converted to virtual slides using Nano Zoomer 2.0 RS
140 (Hamamatsu Photonics Co., Ltd.; Hamamatsu, Japan), and then each measurement was
141 performed using NDP.view2 software (Hamamatsu Photonics Co., Ltd.). The number of MG
142 acini in the upper tarsal plates in the defined area (445 \times 352 μ m) was counted for two areas and
143 expressed as MG acinus density. For the HG, ELG, and ILG, the area of the acinus (1) and its
144 ductal lumen (2) was measured by drawing a line on NDP.view2 (Hamamatsu Photonics Co.,
145 Ltd.); the size of one acinus was obtained by subtracting (2) from (1). This measurement was
146 performed randomly for 50 acini in the HG and ELG, and 30 acini in the ILG, for each sample.
147 For the palpebral conjunctiva, goblet cell density in the conjunctiva epithelium was calculated
148 from the number of goblet cells within the length of two non-overlapping areas from the upper
149 and lower eyelids (more than 500 μ m). We also measured the thickness of the anterior
150 epithelium of the cornea at five points around the central part of the cornea.

151 ***Immunohistochemistry***

152 Paraffin sections were deparaffinized and antigen retrieval was performed. The sections
153 were soaked in methanol containing 0.3% H₂O₂ for 20 min at room temperature to remove
154 internal peroxidase. After washing three times in phosphate buffered saline (PBS), sections were
155 incubated with blocking serum for 1 h at room temperature and primary antibodies overnight at
156 4 °C. Prior to, and after sections were incubated with secondary antibodies for 30 min at room
157 temperature, they were washed three times in PBS. The sections were incubated with
158 streptavidin-conjugated horseradish peroxidase (SABPO(R) kit; Nichirei, Tokyo, Japan) for 30
159 min and washed three times in PBS. For visualisation of the positive reactions, the sections were
160 incubated with 10 mg 3, 3'-diaminobenzidine tetrahydrochloride in 50 mL 0.05 M Tris-HCl
161 buffer-H₂O₂ solution. Finally, sections were stained with haematoxylin. Antibodies, antigen
162 retrieval, and blocking details are listed in Supplementary Table 1.

163

164 ***Scanning electron microscopy (SEM)***

165 Whole eyeball samples from BXSB and BXSB-Yaa at 28 weeks of age were pre-fixed with
166 2.5% glutaraldehyde in 0.1 M phosphate buffer (PB) for 4 h at 4 °C. Then, the samples were
167 washed five times with 0.1 M PB for 10 min each. The samples were post-fixed with 1% OsO₄
168 for 1 h, immersed in 1% tannic acid solution (TAS) for 1.5 h as a conductive treatment, and
169 washed six times with 0.1 M PB for 10 min each at 4 °C. Then, the samples were post-fixed in
170 1% OsO₄ for 1 h again and washed again, as above. Subsequently, the samples were immersed
171 in 0.5% TAS for 10 min and then 1.0% TAS for 1 h at 4 °C. After washing in 0.1 M PB, the
172 specimens were dehydrated with graded ethanol, replaced with isoamyl acetate, and dried using
173 a critical point drier (HCP-2, Hitachi; Tokyo, Japan). The dried specimens were mounted on
174 aluminium stubs, treated by ion sputtering (E-1030, Hitachi), and observed using an SEM (SU
175 8000, Hitachi; 10 kV).

176 ***Statistical analysis***

177 The results are expressed as the mean \pm standard error (SE). Analysis between two groups
178 was conducted using the Mann-Whitney *U*-test. Multiple comparisons over three groups were
179 conducted using Scheffé's method after the Kruskal–Wallis test. The correlation between two
180 parameters was analysed using Spearman's correlation test. In all analyses, $P < 0.05$ was
181 regarded as significantly different.

182 **Results**

183 *Autoimmune disease indices and tear volume*

184 BXSB-Yaa mice at 8, 20, and 28 weeks of age were investigated as models of early, moderate,
185 and late stage autoimmune disease, respectively. BXSB-Yaa showed significantly higher ratios
186 of spleen weight to body weight (S/B) than BXSB at 20 weeks; BXSB-Yaa at 28 weeks showed
187 significantly higher S/B than BXSB-Yaa at 8 weeks (Figure 1A). The serum levels of anti-
188 dsDNA antibody were significantly higher in BXSB-Yaa than in BXSB at all examined weeks
189 without age-related significant differences (Figure 1B). Although BXSB showed no significant
190 age-related changes, tear volume in BXSB-Yaa decreased with age and showed a significant
191 difference between 8 and 20 or 28 weeks (Figure 1C), and a significantly higher value than
192 BXSB at 8 weeks.

193

194 *Histopathology of MG and HG, lipid layer composing exocrine glands*

195 As shown in Figure 2A, MGs are observed as a cluster of foamy sebaceous gland cells
196 beneath the palpebral conjunctiva in the upper or lower tarsal plates. Melanin pigments were
197 observed between the MG acini. No change in acinus morphology was observed among ages or
198 strains, but the number of acini in BXSB-Yaa was lower than that in BXSB at all ages. The HG
199 acini in the third eyelid were composed of clear glandular epithelial cells containing numerous
200 minute lipids in their abundant cytoplasm (Figure 2B). Further, brown-coloured porphyrins were
201 observed in some acinar lumens. No change was observed in porphyrin appearance among ages
202 or strains; the size of acinus decreased from 20 weeks in BXSB-Yaa, but not in BXSB.

203 Inflammatory cell infiltrations in MG and HG were not obvious in all ages of both strains.

204 MG acinar density and HG acinar size in BXSB-Yaa were lower than those in BXSB at 8
205 and 20 weeks (Figure 2C and D); significant strain differences were detected at 28 weeks for
206 both parameters. In BXSB-Yaa, HG values were significantly decreased from 8 weeks to 20 and

207 28 weeks (Figure 2D).

208

209 ***Histopathology of ELG and ILG, water layer composing exocrine glands***

210 Figure 3 shows the histopathological observation of LGs. For ELGs (Figure 3A), serous
211 acini were composed of glandular epithelial cells with a clear and large cytoplasm in the apical
212 portion and a basophilic one in the basal portion. The size of nuclei in acinar epithelial cells or
213 acinar lumens differed among acini, but there was no consistent difference among ages or
214 strains. Although the histological characteristics of ILG were similar to those of ELGs, the ILG
215 acinus was smaller than that of ELG, and the ILG was separated into smaller lobules than the
216 ELG (Figure 3B). No change was observed in ELGs and ILGs of BXSB of all ages, but smaller
217 acini were found in BXSB-Yaa at 20 and 28 weeks than those at 8 weeks.

218 ELG and ILG acinar sizes in BXSB-Yaa were both lower than those in BXSB at 20 weeks,
219 but the reduction in ELG acinar size was significant (Figure 3C and D). In BXSB, the ELG
220 showed increased acinar sizes with age without statistical significance, but in BXSB-Yaa, ILG
221 values significantly decreased from 8 weeks to 20 and 28 weeks (Figure 3D).

222 Since several mononuclear cells are observed between the acini of ELGs, particularly
223 around the ducts, as shown in Figure 3A and previous reports,¹⁷ cell infiltration was evaluated.
224 In all samples, ELGs had cell infiltration at 8, 20, and 28 weeks in BXSB (0/4, 1/4, 2/4 animals,
225 respectively) and BXSB-Yaa (0/4, 4/4, 4/4 animals, respectively). Using immunohistochemistry,
226 these inflammatory cells comprised B220⁺ B-cells, CD3⁺ T-cells, and Iba1⁺ macrophages (Figure
227 4A-C). For ILG, cell infiltration was scarce, but one sample from BXSB-Yaa at 20 weeks (1/4
228 animals) showed cell infiltration. These lesions comprised B220⁺ B-cells, CD3⁺ T-cells, and
229 Iba1⁺ macrophages, similar to ELG (Figure 4D).

230

231 ***Histopathology of goblet cells in the palpebral conjunctiva and mucin layer composing cells***

232 In all mice, the palpebral or forniceal conjunctiva was composed of stratified cuboidal to

233 columnar epithelium (Figure 5A). Several PAS-positive goblet cells were observed in the
234 epithelium of the palpebral or forniceal conjunctiva. For the palpebral conjunctiva, there was no
235 morphological difference between the upper and lower eyelids. In BXSB, the number of PAS⁺
236 palpebral conjunctiva goblet cells decreased at 20 and 28 weeks compared to those at 8 weeks.
237 Goblet cell numbers also decreased in BXSB-Yaa from 8 to 20 weeks but increased again at 28
238 weeks. Figure 5B shows the goblet cell density in the palpebral conjunctiva. In BXSB-Yaa,
239 PAS⁺ conjunctiva goblet cells significantly decreased from 8 to 20 weeks but increased from 20
240 to 28 weeks, without statistical significance. At 28 weeks, BXSB-Yaa showed significantly
241 higher values than BXSB.

242

243 *Histopathology of the cornea*

244 The cornea is composed of the anterior epithelium, the proper substance, the posterior
245 limiting membrane (Descemet's membrane), and the posterior epithelium from the outside, as
246 shown in Figure 6A. The anterior epithelium is stratified squamous epithelium with 5-7 cell
247 layers, which is influenced by changes in the tear film,³² and it thickened with ageing in BXSB,
248 but not in BXSB-Yaa (Figure 6A). BXSB, but not BXSB-Yaa, had significantly increased
249 thickness of the anterior corneal epithelium from 8 weeks to 20 weeks, but the epithelium in
250 BXSB-Yaa was significantly thinner than that in BXSB at 28 weeks (Figure 6B).

251 SEM analysis of the ultrastructure of the corneal surface was performed in BXSB and
252 BXSB-Yaa at 28 weeks (Figure 6C). Under low magnification, BXSB showed a smooth and flat
253 surface while BXSB-Yaa showed a few dark areas. High magnification analysis revealed that
254 the surface of the cornea was covered by numerous microvilli in BXSB, but the dark area,
255 observed under low magnification, lacked intact microvilli in 75% of examined BXSB-Yaa
256 (n=4).

257

258 *Correlation among tear volume, autoimmune disease indices, and altered tear-secreting*

259 *tissue morphologies*

260 The correlations among tear volumes, the indices of autoimmune disease, and tear-
261 secreting tissue morphologies are summarised in Table 1. For all mice, tear volume showed no
262 correlations with any parameters, but S/B and anti-dsDNA antibody were significantly and
263 negatively correlated with MG and HG histological parameters. S/B also correlated with ELG
264 and ILGs, indicating the relationship between autoimmune disease development and
265 histopathological alterations.

266 BXSB-Yaa tear volume was significantly and positively correlated with ILG histological
267 parameters, and S/B significantly and negatively correlated with HG and ILG histological
268 parameters, as well as tear volume, showing age-related decreases in this strain. This result
269 correlates autoimmune disease progression with alteration of tear volume and morphological
270 changes in these organs. Moreover, our correlation analysis revealed that corneal
271 histopathological parameter was only significantly and negatively correlated with conjunctival
272 goblet cells in all mice and BXSB-Yaa mice (Supplemental Table 1).

273 **DISCUSSION**

274 BXSB-Yaa showed increased serum levels of anti-dsDNA antibody and S/B from 8 to 20
275 weeks, indicating the onset of autoimmune abnormality started from 8 weeks. Although the tear
276 volume index decreased with age in BXSB-Yaa, these mice showed higher values than BXSB at
277 8 weeks. The Schirmer test paper indicated basal as well as reflex secretion of tears due to the
278 physical stimuli of paper insertion into the conjunctival sac.²² Therefore, the altered tear volume
279 in BXSB-Yaa suggested a change in basal and/or reflex secretion from tear-producing
280 components. At 8 weeks, there was no significant difference in the tear film- or cornea-
281 associated histoplanimetry between the two strains, but BXSB-Yaa showed a lower MG acinar
282 density, an important component forming the tear film lipid layer. Tear volume increases to
283 compensate for the decreased lipid layer in stearoyl coenzyme A desaturase-1 (SCD-1) deficient
284 mice, which lack the enzyme related to lipid synthesis and suffer from MG dysfunction.³³ Tear
285 volume and autoimmune indices were significantly and negatively correlated in BXSB-Yaa.
286 Thus, we hypothesised that tear volume increased to compensate for the decreased lipid layer
287 from MG dysfunction in young BXSB-Yaa and decreased with the progression of autoimmune
288 disease and the altered function of tear film-producing organs.

289 In aged BXSB-Yaa (middle and late stage), altered acinar morphology was observed in
290 ELG and ILG, the water layer-producing components. Cell infiltration in these LGs was
291 observed in BXSB-Yaa but not in BXSB. The destruction of LGs and salivary glands in SS
292 model mice is mediated by cytokines, such as interleukins or interferons, secreted from
293 infiltrating lymphocytes.³⁴ In BXSB-Yaa, the histological changes in ILG, but not ELG,
294 significantly correlated with tear volume and S/B, suggesting the close relationship with altered
295 ILG morphology and autoimmune disease or tear production in mice, although ELG showed
296 more cell infiltration than ILG. Only the LGs, but not other organs, showed obvious
297 inflammatory features, even though HG and MG morphology was altered in ageing BXSB-Yaa.

298 Thus, lipid- and water layer-producing organs showed different pathological processes; further
299 study is needed to elucidate the mechanism. Moreover, clarification of cellular cluster around
300 the duct as tertiary lymphoid cluster might add value to identify the pathogenesis of
301 histomorphological changes of LG.

302 Age-related changes in HG, ELG, ILG and conjunctiva goblet cell histopathological
303 indices in BXS_B-Yaa at 20 weeks indicated their altered morpho-function, assuming they were
304 associated with tear film stability. While the anterior corneal epithelium thickened from 8 to 20
305 weeks in both strains, it was thinner in BXS_B-Yaa than in BXS_B at 28 weeks. Consistent with
306 our results, the anterior corneal epithelium thickens with ageing in healthy mice,³⁵ and dry eye
307 model mice have thinner corneal epithelium due to cell injuries than healthy controls.¹⁰ Previous
308 study showed that tear film instability potential damaged to the ocular surface.³² Our SEM data
309 also revealed that several areas on the corneal surface lacked microvilli in aged-BXS_B-Yaa,
310 which might reflect corneal injury at 28 weeks due to the unstable tear film.

311
312 The density of conjunctiva goblet cells and mucin layer-associated cells decreased from 20
313 weeks in BXS_B. Conjunctival goblet cell density decreases in healthy mice with ageing.³⁶ Cell
314 density in BXS_B-Yaa decreased from 8 to 20 weeks but recovered at 28 weeks. At 28 weeks, the
315 BXS_B-Yaa group developed prominent autoimmune disease abnormalities that significantly
316 altered tear film-producing organs, including MG, HG, ILG, and the cornea. Moreover,
317 inflammatory cytokines associated with SS contributes to dry eye by inducing apoptosis and
318 increasing mucin secretion and conjunctival goblet cell proliferation.³⁷ Therefore, we
319 hypothesised that increased goblet cells in BXS_B-Yaa at 28 weeks compensated for their altered
320 morpho-function. In fact, SCD-1 deficient mice, which exhibit MG dysfunction, show a
321 compensatory increase in mucin levels in their tears.³³ Our correlation analysis revealed that
322 conjunctival goblet cells and corneal histopathological parameters showed significant and
323 negative correlations in all mice ($\rho=-0.685$, $P < 0.01$) and BXS_B-Yaa ($\rho=-0.748$, $P < 0.01$),

324 supporting this compensation theory.

325 Here, BXSB-Yaa satisfied at least two of the Japanese SS diagnostic criteria: lymphocytic
326 infiltration in LGs and corneal injury. Therefore, BXSB-Yaa could be a model for SS-like
327 disease, even if lacrimal hyposalivation did not develop. SS-like disease in model mice
328 progresses according to three phases.³⁸ Phase 1 shows increased apoptosis of acinar cells and
329 abnormal protein or gene expression. Phase 2 shows inflammatory cell infiltration into the
330 exocrine gland and autoantibody production. Phase 3 shows loss of secretory function
331 progression, as found in dry eye. Based on this study, and another,²² BXSB-Yaa developed
332 phase 2 SS. This autoimmune disease-prone strain would likely develop dry eye because tear
333 volume significantly decreases with ageing in these mice.

334 In conclusion, we demonstrated that systemic autoimmune abnormality in BXSB-Yaa was
335 associated with histological changes in the exocrine glands and cornea of the eyes. Thus,
336 BXSB-Yaa could be a model for mild stage SS-like disease-associated dry eye. Further studies
337 focusing on the cause of morphological or detailed functional changes in tear-secreting glands
338 would elucidate the pathology of SS-associated symptoms in human and veterinary medicine.

339 **Authors' contributions**

340 M.H., M.A. M., T. N., Y. O., Y. H. A. E, O.I., and Y.K. designed and performed experiments.

341 M.H. and M.A. M. analysed the data. All authors were involved in writing the paper and

342 approved the final manuscript.

343 **Acknowledgement**

344 This research was awarded the Encouragement Award (undergraduate section) at the 162nd

345 Japanese Association of Veterinary Anatomists in Tsukuba, Japan (September 2019).

346

347 **Declaration of conflicting interests**

348 The authors declared no potential of interest with respect to the research, authorship, and/or

349 publication of this article.

350

351 **Funding**

352 This research received no specific grant from any funding agency in the public, commercial, or

353 not-for-profit sectors.

354 **FIGURE LEGENDS**

355 **Figure 1. Indices for autoimmune abnormality and tear volume in mice.**

356 (A) The ratio of spleen weight to body weight.

357 (B) The serum levels of anti-double stranded DNA (dsDNA) antibody.

358 (C) Tear volume

359 BXSB: BXSB/MpJ. BXSB-Yaa: BXSB/MpJ-*Yaa*. Each bar represents the mean \pm SE (n = 4).

360 *: Significant strain difference at the same age, Mann-Whitney *U*-test. †: Significant difference
361 from the other groups, Kruskal-Wallis test followed by Scheffe's method.

362

363 **Figure 2. Histopathology of lipid layer-composing exocrine glands in mice.**

364 (A) Meibomian glands (MGs) in the upper tarsal plate. Sebaceous gland cells form clusters
365 beneath the conjunctival epithelium (CE). Melanin pigments indicated by arrowheads are
366 observed between and around acinar cells. CS: conjunctival sac. Cor: Cornea. HE staining.
367 Bars = 100 μ m.

368 (B) Harderian glands (HGs) in the third eyelid. Acini of HGs are composed of clear glandular
369 epithelial cells containing numerous minute lipids in their abundant cytoplasm. Some acini
370 include porphyrins in their lumens. Arrowheads point to porphyrin. Smaller acinar
371 epithelial cells are observed in BXSB-Yaa at 20 and 28 weeks. HE staining. Bars = 100
372 μ m.

373 (C) MG acinus density.

374 (D) The size of one acinus in HGs.

375 BXSB: BXSB/MpJ. BXSB-Yaa: BXSB/MpJ-*Yaa* Each bar represents the mean \pm SE (n = 4).

376 *: Significant strain difference at the same age, Mann-Whitney *U*-test. †: Significant difference
377 from the other groups, Kruskal-Wallis test followed by Scheffe's method.

378

379 **Figure 3. Histopathology of water layer-composing exocrine glands in mice.**

380 (A) Extraorbital lacrimal glands (ELGs). Each acinus is composed of serous cells and a small
381 lumen. Mononuclear cells (arrowheads) are observed around the ducts (arrows). Smaller
382 acini are observed in BXS_B-Yaa at 20 and 28 weeks. HE staining. Bars = 100 μm.

383 (B) Intraorbital lacrimal glands (ILGs). Histological characteristics are similar to those of ELG.
384 These glands are separated into smaller lobules. Smaller acini are observed in BXS_B-Yaa at
385 20 and 28 weeks. HE staining. Bars = 100 μm.

386 (C) Size of one acinus in ELGs.

387 (D) Size of one acinus in ILGs.

388 BXS_B: BXS_B/MpJ. BXS_B-Yaa: BXS_B/MpJ-*Yaa* Each bar represents the mean ± SE (n = 4). *
389 *: Significant strain difference at the same age, Mann-Whitney *U*-test. †: Significant difference
390 from the other groups, Kruskal-Wallis test followed by Scheffe's method.

391

392 **Figure 4. Inflammatory cell infiltration in lacrimal glands.**

393 (A-C) Immunohistochemistry for B220 (panel A), CD3 (panel B), and Iba1 (panel C) in
394 extraorbital lacrimal glands. Positive cells localise around the ducts (arrowheads). Bars =
395 100 μm.

396 (D) Immunohistochemistry for B220, CD3, and Iba1 in intraorbital lacrimal glands in BXS_B-
397 Yaa at 20 weeks of age. Bars = 100 μm.

398

399 **Figure 5. Histopathology of mucin layer-producing tissues in mice.**

400 (A) Palpebral conjunctiva in the upper or lower eyelids. PAS⁺ goblet cells, indicated by
401 arrowheads, are observed in the epithelium of the palpebral conjunctiva. The number of
402 goblet cells decreased in BXS_B with age, but not in BXS_B-Yaa. PAS staining. Bars = 100
403 μm. CS: Conjunctival sac.

404 (B) Goblet cell density in the conjunctival epithelium.

405 BXS_B: BXS_B/MpJ. BXS_B-Yaa: BXS_B/MpJ-*Yaa* Each bar represents the mean ± SE (n = 4). *

406 *: Significant strain difference at the same age, Mann-Whitney *U*-test. †: Significant difference
407 from the other groups, Kruskal-Wallis test followed by Scheffe's method.

408

409

410 **Figure 6. Histopathology of cornea in mice.**

411 (A) Cornea histology. The cornea is composed of four layers: the anterior epithelium (AE), the
412 proper substance (PS), Descemet's membrane (DM), and the posterior epithelium (PE).

413 The anterior epithelia of the cornea thickened with age in BXSB, but not in BXSB-Yaa. HE
414 staining. Bars (black) = 100 μ m. Bars (inset) = 20 μ m.

415 (B) Thickness of corneal AE.

416 (C) Scanning electron microscopy images of the anterior surface of the cornea. Numerous
417 microvilli cover the surface of the cornea in BXSB, and they disappear in some areas in
418 BXSB-Yaa at 28 weeks of age. The area without microvilli is surrounded by a dotted line.

419 Bars = 5 μ m

420 BXSB: BXSB/MpJ. BXSB-Yaa: BXSB/MpJ-Yaa Each bar represents the mean \pm SE (n = 4). *

421 *: Significant strain difference at the same age, Mann-Whitney *U*-test. †: Significant difference
422 from the other groups, Kruskal-Wallis test followed by Scheffe's method.

423

424

425

426

427 **REFERENCES**

- 428 1. Walcott B. The lacrimal gland and its veil of tears. *News Physiol Sci* 1998; **13**: 97-103.
- 429 2. Shinomiya K, Ueta M and Kinoshita S. A new dry eye mouse model produced by exorbital
430 and intraorbital lacrimal gland excision. *Sci Rep* 2018; **8**: 1483.
- 431 3. Foulks GN and Bron AJ. Meibomian gland dysfunction: A clinical scheme for description,
432 diagnosis, classification, and grading. *Ocul Surf* 2003; **1**: 107–126.
- 433 4. Payne AP. The harderian gland: a tercentennial review. *J Anat* 1994; **185**: 1–49.
- 434 5. Barbosa FL, Xiao Y, Bian F, Coursey TG, Ko BY, Clevers H, de Paiva CS and Pflugfelder
435 SC. Goblet cells contribute to ocular surface immune tolerance—implications for dry eye
436 disease. *Int J Mol Sci* 2017; **18**: pii: E978.
- 437 6. Ralph RA. Conjunctival goblet cell density in normal subjects and in dry eye syndromes.
438 *Invest Ophthalmol* 1975; **14**: 299–302.
- 439 7. Mishima S and Maurice DM. The oily layer of the tear film and evaporation from the
440 corneal surface. *Exp Eye Res* 1961; **1**: 39–45.
- 441 8. Cui X, Hong J, Wang F, Deng SX, Yang Y, Zhu X, Wu D, Zhao Y and Xu J. Assessment
442 of corneal epithelial thickness in dry eye patients. *Optom Vis Sci* 2014; **91**: 1446–1454.
- 443 9. Dodi P. Immune-mediated keratoconjunctivitis sicca in dogs: current perspectives on
444 management. *Vet Med (Auckl)* 2015; **6**: 341-347.
- 445 10. Marques DL, Alves M, Modulo CM, da Silva LECM, Reinach P and Rocha EM. Lacrimal
446 osmolaritu and ocular surface in experimental model of dry eye caused by toxicity. *Rev*
447 *Bras Oftalmol* 2015; **74**: 68–72.
- 448 11. Alves M, Novaes P, Morraye MdeA, Reinach PS and Rocha EM. Is dry eye an
449 environmental disease? *Arq Bras Oftalmol* 2014; **77**: 193–200.
- 450 12. Stevenson W, Chauhan SK and Dana R. Dry eye disease: and immune-mediated ocular
451 surface disorder. *Arch Ophthalmol* 2012; **130**: 90-100.
- 452 13. Toda I. Dry eye after lasik. *Invest Ophthalmol Vis Sci* 2018; **59**: 109–115.

- 453 14. Wilkinson BR. Dry eye syndrome. *Ophthalmology* 1999; **106**: 1044.
- 454 15. Sjogren H. Keratoconjunctivitis sicca and chronic polyarthritis. *Acta Med Scand* 1948; **130**:
455 484-488.
- 456 16. Helmick CG, Felson DT, Lawrence RC, Gabriel S, Hirsch R, Kwoh CK, Liang MH,
457 Kremers HM, Mayes MD, Merkel PA, Pillemer SR, Reveille JD and Stone JH. Estimates
458 of the prevalence of arthritis and other rheumatic conditions in the United States. *Arthritis*
459 *Rheum* 2008; **58**: 15-25.
- 460 17. Ambrosetti A, Zanotti R, Pattaro C, Lenzi L, Chilosi M, Caramaschi P, Arcaini L, Pasini F,
461 Biasi D, Orlandi E, D'Adda M, Lucioni M and Pizzolo G. Most cases of primary salivary
462 mucosa-associated lymphoid tissue lymphoma are associated either with Sjogren
463 syndrome or hepatitis C virus infection. *Br J Haematol* 2004; **126**: 43-49.
- 464 18. de Vita S, Boiocchi M, Sorrentino D, Carbone A, Avellini C, Dolcetti R, Marzotto A,
465 Gloghini A, Bartoli E, Beltrami CA and Ferraccioli G. Characterization of
466 prelymphomatous stages of B cell lymphoproliferation in Sjogren's syndrome. *Arthritis*
467 *Rheum* 1997; **40**: 318-331.
- 468 19. Voulgarelis M and Moutsopoulos HM. Lymphoproliferation in autoimmunity and
469 Sjogren's syndrome. *Cur Rheum Rep* 2003; **5**: 317-32.
- 470 20. Nabeta R, Kambe N, Nakagawa Y, Chiba S, Xiantao H, Feruya T, Kishimoto M and
471 Uchida T. Sjogren's-like syndrome in a dog. *J Vet Med Sci* 2019; **81**: 886-889.
- 472 21. Quimby FW, Schwartz RS, Poskitt T and Lewis RM. A disorder of dogs resembling
473 Sjogren's syndrome. *Clin Immunol Immunopathol* 1979; **12**: 471-476.
- 474 22. Kosenda K, Ichii O, Otsuka S, Hashimoto Y and Kon Y. BXSB/MpJ-Yaa mice develop
475 autoimmune dacryoadenitis with the appearance of inflammatory cell marker messenger
476 RNAs in the lacrimal fluid. *Clin Exp Ophthalmol* 2013; **41**: 788-97.
- 477 23. Payne AP. The Harderian gland: a tercentennial review. *J Anat* 1994; **185**: 1-49.
- 478 24. Hoffman RW, Alspaugh MA, Waggle KS, Durham JB and Walker SE. Sjogren's

- 479 Syndrome in MRL/l and MRL/n mice. *Arthritis Rheum* 1984; **27**: 157-65.
- 480 25. Sullivan DA, Dana R, Sullivan RM, Krenzer KL, Sahin A, Arica B, Liu Y, Kam WR,
481 Papas AS and Cermak JM. Meibomian gland dysfunction in primary and secondary
482 Sjögren Syndrome. *Ophthalmic Res* 2018; **59**: 193–205.
- 483 26. Wang C, Zaheer M, Bian F, Quach D, Swennes AG, Britton RA, Pflugfelder SC and de
484 Paiva CS. Sjögren-like lacrimal keratoconjunctivitis in germ-free mice. *Int J Mol Sci* 2018;
485 **19**: 565.
- 486 27. Williamson J, Gibson AA, Wilson TH, Forrester JV, Whaley KB and Dick WC. Histology
487 of the lacrimal gland in keratoconjunctivitis sicca. *Br J of Ophthalmol* 1973; **57**: 852–858.
- 488 28. Jabs DA, Alexander EL and Green WR. Ocular inflammation in autoimmune MRL/Mp
489 mice. *Invest Ophthalmol Vis Sci* 1985; **26**: 1223–1229.
- 490 29. Haywood ME, Rogers NJ, Rose SJ, Boyle J, McDermott A, Rankin JM, Thirudaian V,
491 Lewis MR, Fossati-Jimack L, Izui S, Walport MJ and Morley BJ. Dissection of BXSB
492 lupus phenotype using mice congenic for chromosome 1 demonstrates that separate
493 intervals direct different aspects of disease. *J Immunol* 2004; **173**: 4277–4285.
- 494 30. Kimura J, Ichii O, Otsuka S, Sasaki H, Hashimoto Y and Kon Y. Close relations between
495 podocyte injuries and membranous proliferative glomerulonephritis in autoimmune murine
496 models. *Am J Nephrol* 2013; **38**: 27–38.
- 497 31. Pisitkun P, Deane JA, Difilippantonio MJ, Tarasenko T, Satterthwaite AB and Balland S.
498 Autoreactive B cell responses to RNA-related antigens due to TLR7 gene duplication.
499 *Science* 2006; **312**: 1669–1672.
- 500 32. Lam H, Bleiden L, de Paiva CS, Farley W, Stern ME and Pflugfelder SC. Tear cytokine
501 profiles in dysfunctional tear syndrome. *Am J Ophthalmol* 2009; **147**: 198-205.
- 502 33. Inaba T, Tanaka Y, Tamaki S, Ito T, Ntambi JM and Tsubota K. Compensatory increases
503 in tear volume and mucin levels associated with meibomian gland dysfunction caused by
504 stearyl-CoA desaturase-1 deficiency. *Sci Rep* 2018; **8**: 3358.

- 505 34. Hayashi T. Dysfunction of lacrimal and salivary glands in Sjögren's syndrome:
506 Nonimmunologic injury in preinflammatory phase and mouse model. *J Biomed Biotechnol*
507 2011; **2011**: 407431.
- 508 35. Inomata T, Mashaghi A, Hong J, Nakao T and Dana R. Scaling and maintenance of corneal
509 thickness during aging. *PLoS One* 2017; **12**: e0185694.
- 510 36. Volpe EA, Henriksson JT, Wang C, Barbosa FL, Zaheer M, Zhang X, Pflugfelder SC and
511 de Paiva CS. Interferon-gamma deficiency protects against aging-related goblet cell loss.
512 *Oncotarget* 2016; **7**: 64605–64614.
- 513 37. Contreras-Ruiz L, Ghosh-Mitra A, Shatos MA, Dartt DA and Masli S. Modulation of
514 conjunctival goblet cell function by inflammation cytokines. *Mediators Inflamm* 2013; **2013**:
515 636812.
- 516 38. Lee BH, Tudares MA and Nguyen CQ. Sjögren's syndrome: An old tale with a new twist.
517 *Arch Immunol Ther Exp* 2009; **57**: 57–66.

1 Table 1. Correlations among tear volume, autoimmune disease indices, and altered tear-secreting tissue morphologies.

			Tear volume	Lipid		Water		Mucin	Cornea
				MG	HG	ELG	ILG	Conjunctiva	
All	Tear volume	ρ	1.000	-0.219	0.161	-0.009	0.323	-0.050	0.015
		P	-	0.304	0.453	0.968	0.124	0.816	0.944
	S/B	ρ	-0.184	-0.481*	-0.591**	-0.418*	-0.475*	0.176	-0.157
		P	0.391	0.017	0.002	0.042	0.019	0.412	0.465
	Anti-dsDNA antibody	ρ	-0.085	-0.619**	-0.436*	-0.388	-0.286	-0.109	-0.117
		P	0.694	0.001	0.033	0.061	0.175	0.612	0.588
BXSB-Yaa	Tear volume	ρ	1.000	-0.360	0.455	0.161	0.587*	-0.098	-0.077
		P	-	0.25	0.138	0.618	0.045	0.762	0.812
	S/B	ρ	-0.930**	0.322	-0.664*	-0.315	-0.608*	0.119	0.182
		P	0	0.308	0.018	0.319	0.036	0.713	0.572
	Anti-dsDNA antibody	ρ	-0.657*	0.265	-0.126	-0.224	-0.545	-0.420	0.420
		P	0.02	0.405	0.697	0.484	0.067	0.175	0.175

2

3 Spearman's rank correlation coefficients *: $P < 0.05$, **: $P < 0.01$.

4 All mice (n = 24), BXSB-Yaa: BXSB/MpJ-Yaa (n = 12)

5 S/B: The ratio of spleen weight to body weight, Tear: Tear volume, MG: MG acinus density, HG: The size of one acinus in the Harderian gland,

6 ELG: The size of one acinus in the extraorbital lacrimal gland, ILG: The size of one acinus in the intraorbital lacrimal gland, Conjunctiva: The goblet

7 cell density in the conjunctiva epithelium; Cornea: the thickness of the corneal anterior epithelium; -: not determined.

8

Figure 1

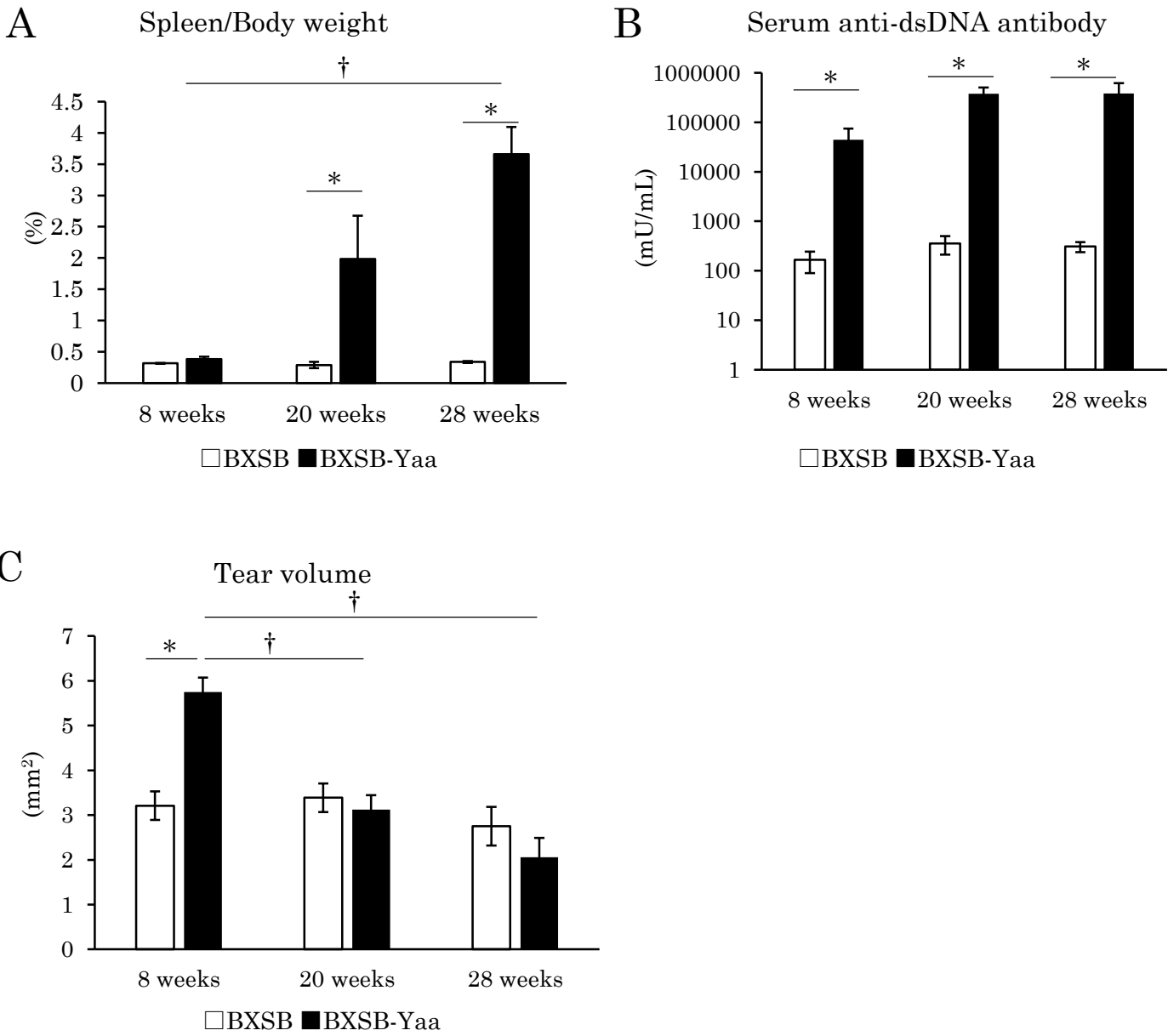


Figure. 2

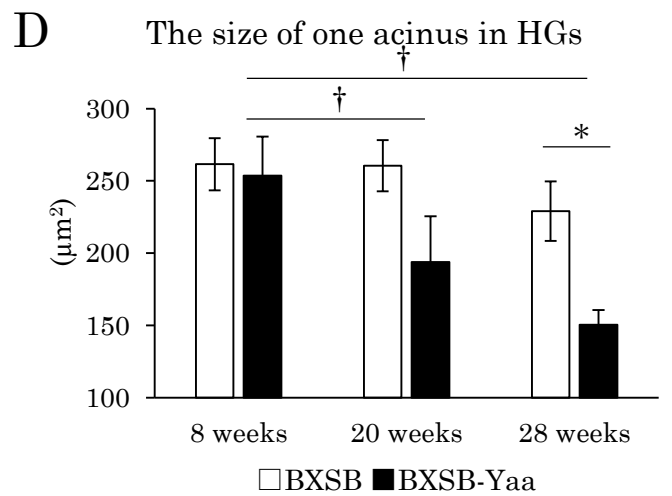
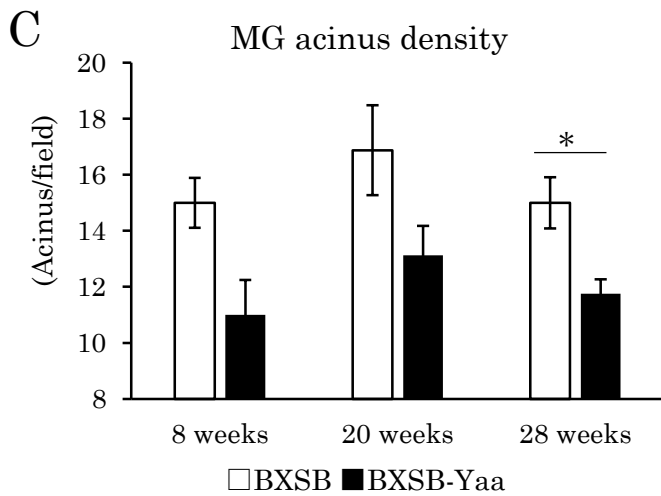
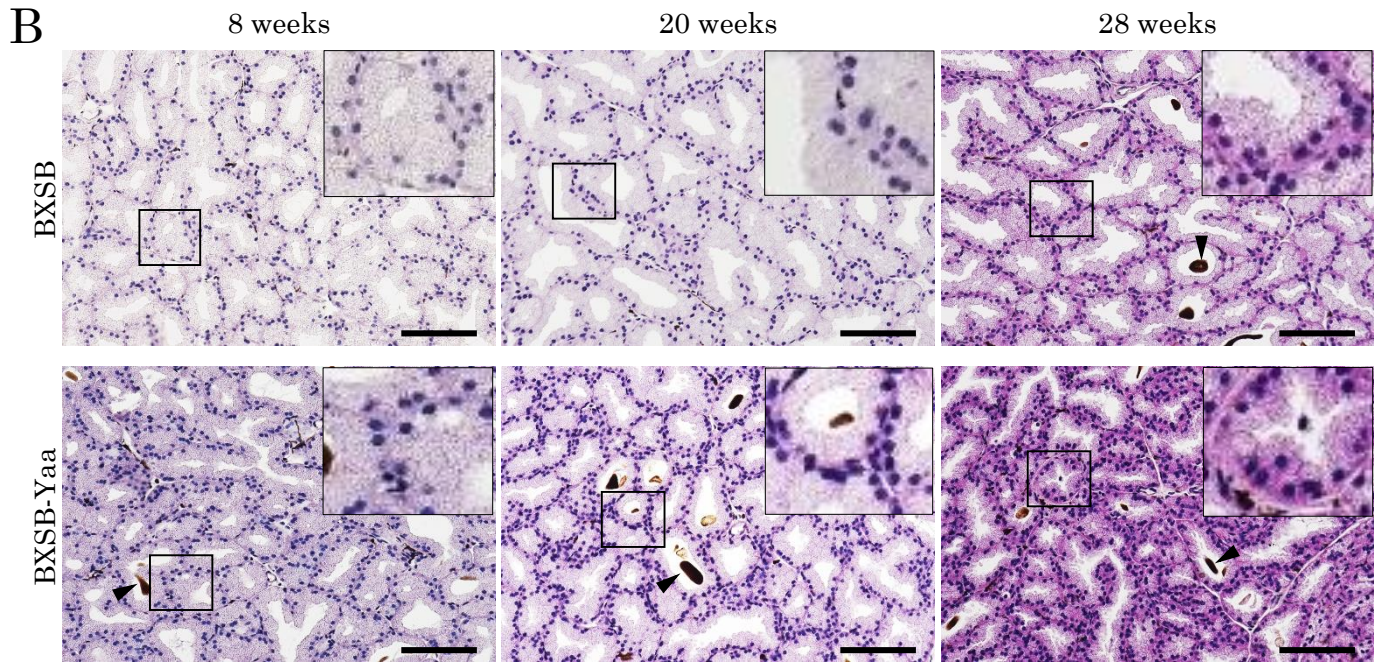
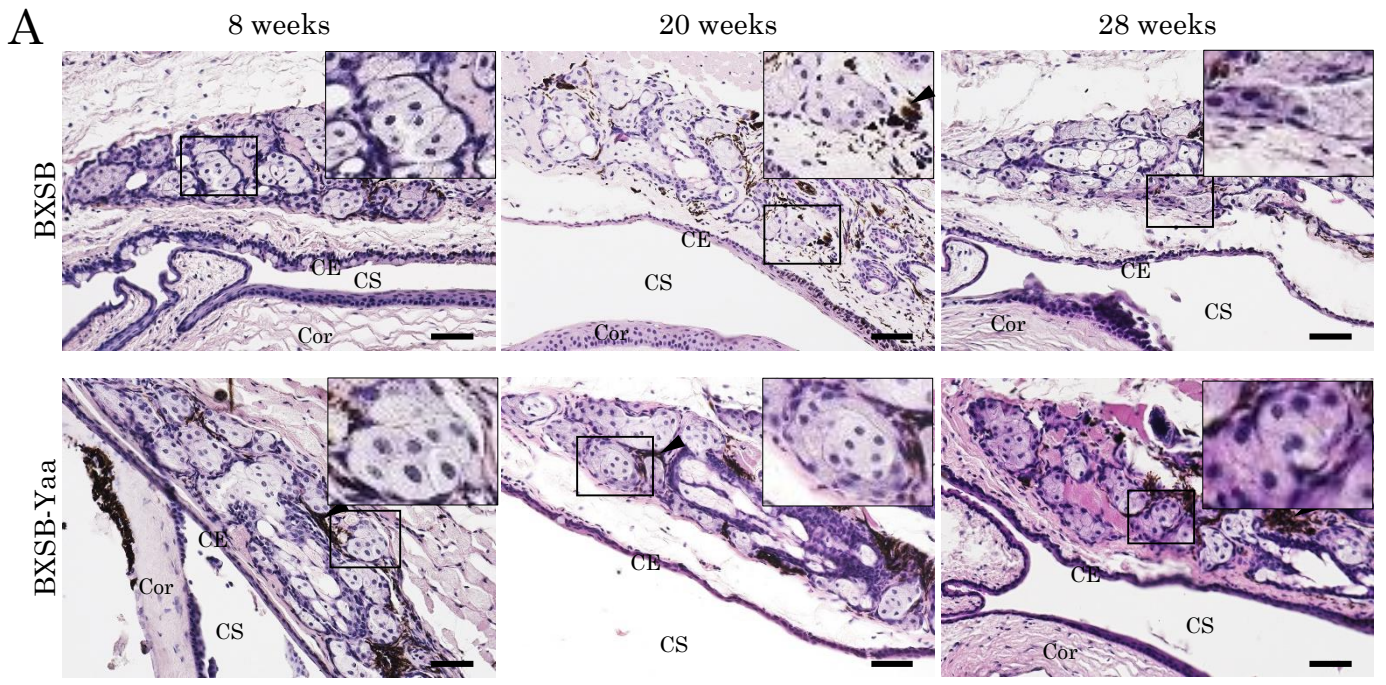


Figure. 3

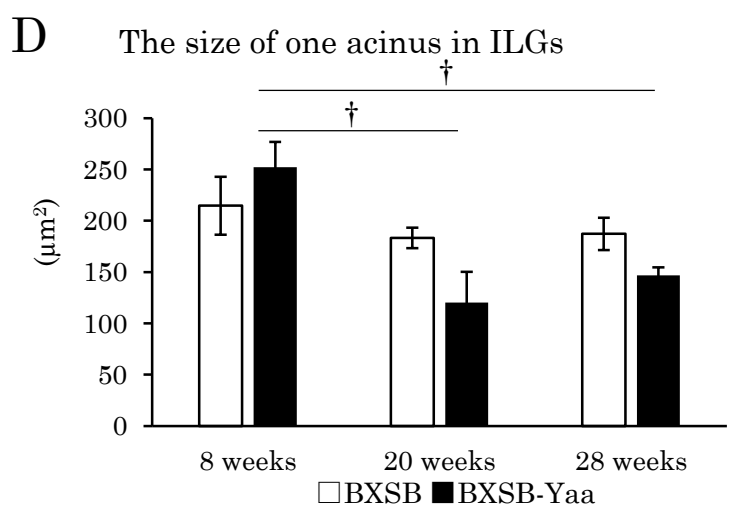
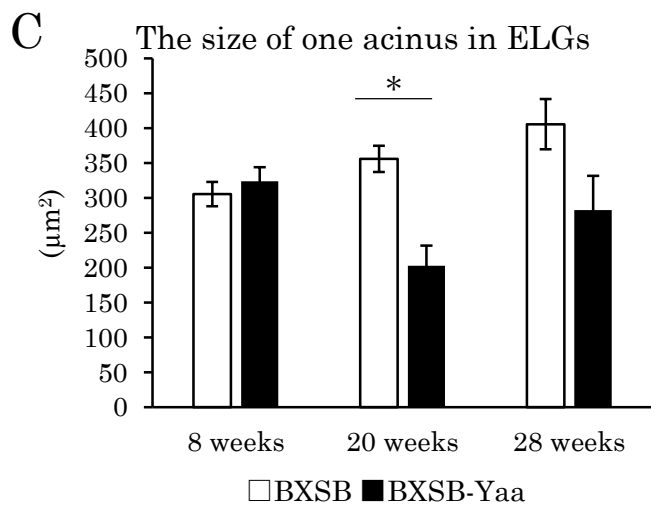
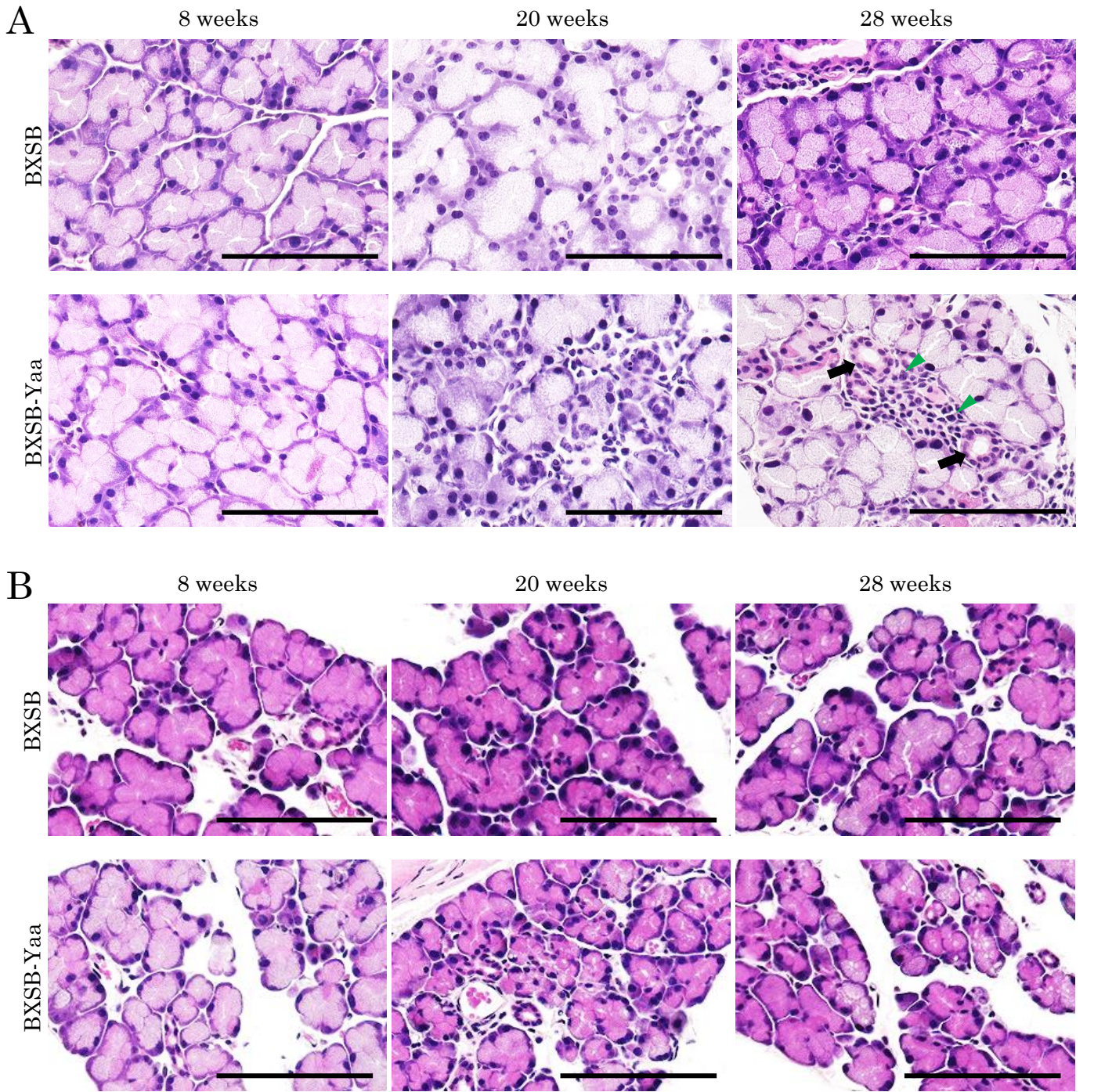


Figure. 4

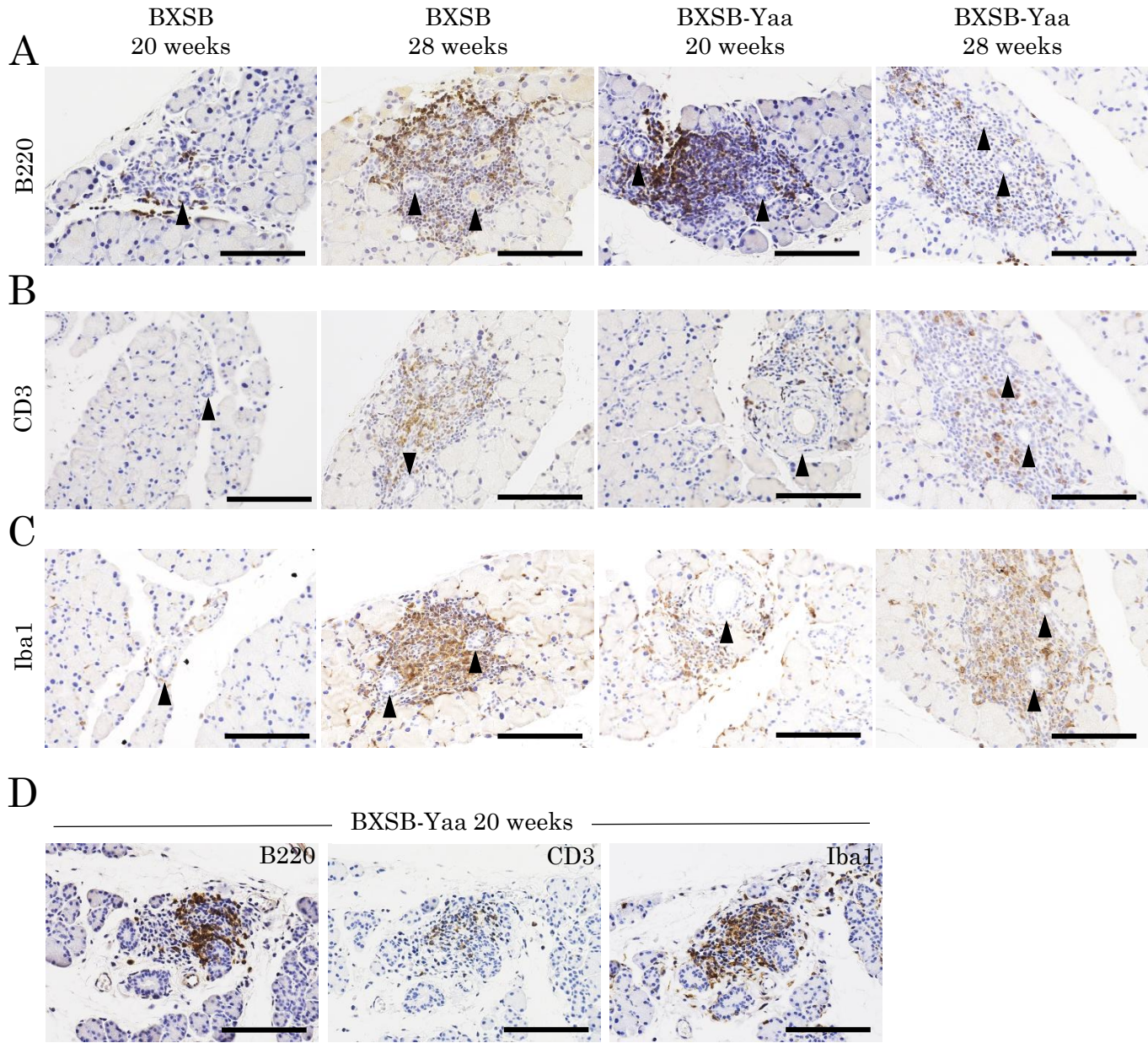
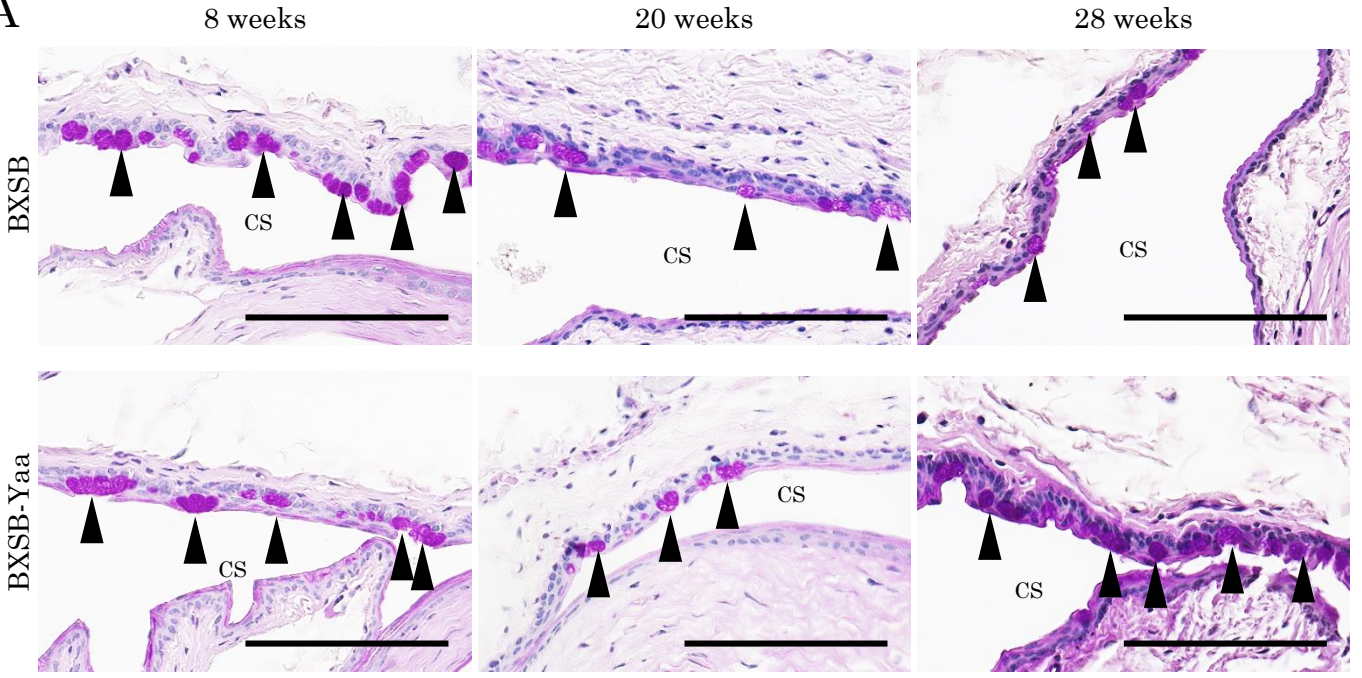


Figure. 5

A



B

Goblet cell density

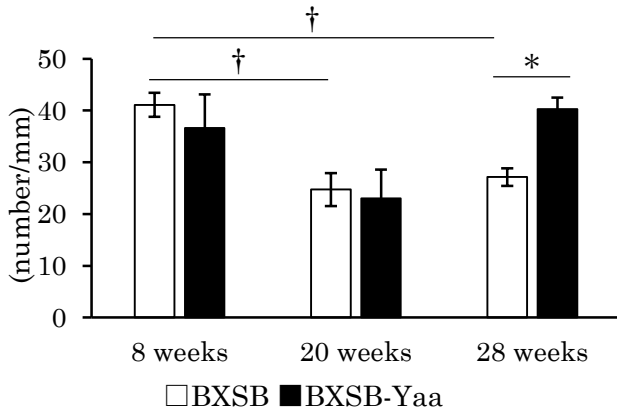
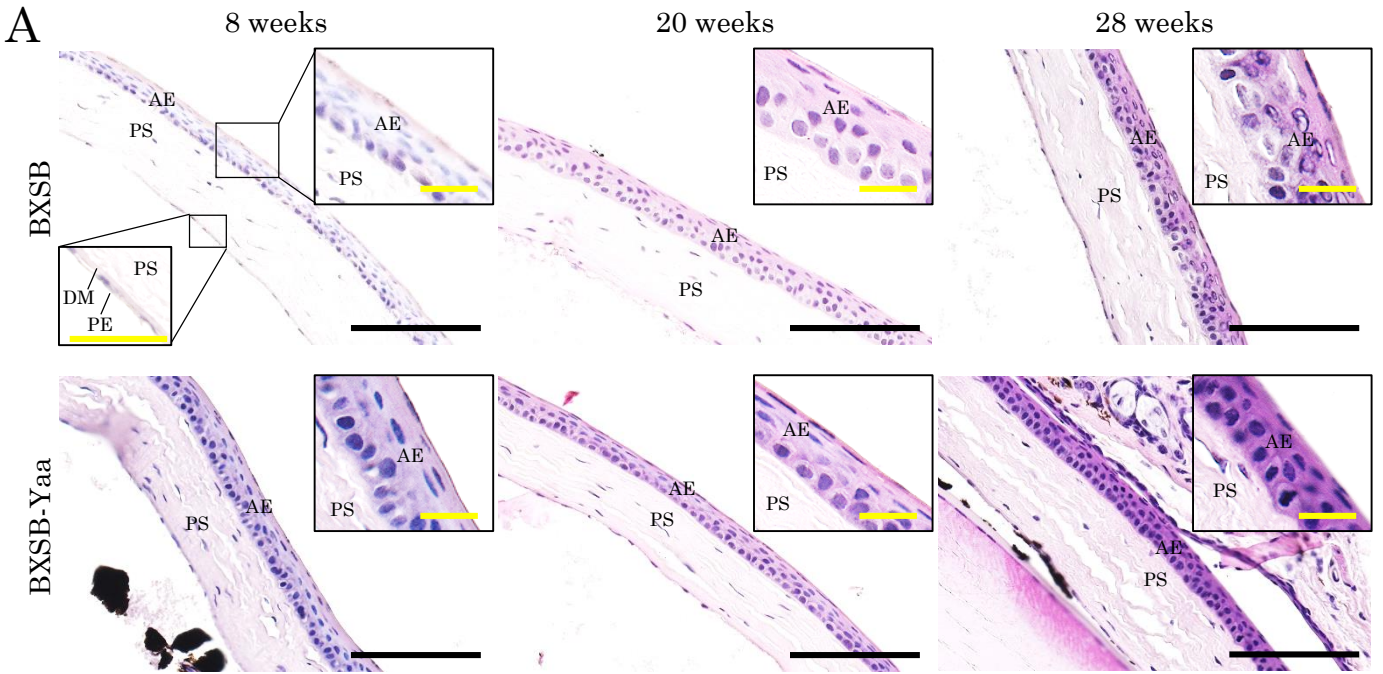


Figure. 6



B Thickness of cornea anterior epithelium

